Influence of SO_3 and MgO on Clinker Mineralogical Composition: an "in-situ" HTXRD Study

M. Marchi[1], U. Costa[1], G. Artioli[2]

[1]CTG –Italcementi Group, Bergamo, Italy; [2]University of Milan, Milan, Italy

1 Introduction

X-ray diffraction (XRD) is a widely used technique for studying phase equilibrium in ceramic systems. The traditional experimental approach consists of an isothermal burning of the mixture followed by quenching. A mineralogical analysis, including XRD, is then carried out on the sintered material.

A more rigorous approach, consisting in the measurement of the crystallographic properties of matter when various temperature or pressure conditions are applied upon the sample, is performed by the so-called “in situ” techniques. XRD can be directly performed on conditioned samples offering a number of advantages over the traditional procedure, insofar as: (a) The structural changes are directly probed at the selected condition and no assumption is made on the preservation of the structural properties upon quenching; (b) The chemical transformations occurring in the raw mixture at short time intervals can be detected during dynamic or static heating treatment by using fast detectors or more brilliant X-ray sources (such as synchrotron radiation).

The aim of the present work was to validate the use of “in-situ” High Temperature X-Ray Powder Diffraction (HTXRPD) experiments for studying phase diagrams of interest to the cement industry.

A further objective was to experimentally confirm the empirical correlation between chemical composition parameters and mineralogical composition as found in clinker samples [4].

The study entailed three experiments as follows: (1) The determination of the phase composition modifications during the cooling process from 1500 °C to 1200 °C of mixtures representing typical clinker composition in the basic CaO-SiO_2-Al_2O_3-Fe_2O_3 system; (2, 3) The determination of the influence of SO_3 and MgO on the phase equilibrium by carrying out similar experiments on the same basic mixtures with appropriate doping.

The results of HTXRPD experiments were compared with those obtained by traditional quenching and with those known from the literature [2,3].

2 Experimental

2.1 Sample preparation

Mixtures of 4N-grade chemical reagents were prepared starting from pure $CaCO_3$ (99.94% - Merck), SiO_2 (99.90% - Merck), Al_2O_3 (98.5% - Carlo Erba) and Fe_2O_3 (99.9% - Carlo Erba). For SO_3 and MgO bearing samples, mixtures of the above four chemical reagents plus $CaSO_4$ $2H_2O$ (99% - Carlo Erba) and MgO (99% - Carlo Erba) respectively were prepared.
Three basic mixtures were prepared with three different Al_2O_3 to Fe_2O_3 ratios - 1.15, 1.38 and 2.0 respectively - to represent the cases of initial liquid composition above, at and below the invariant point at 1338°C of the pseudo-system CaO-C_2S-$C_{12}A_7$-C_4AF [5].
The SO_3 and MgO content in the sintered materials ranged from 0 to 1.5 wt%. The chemical composition of the mixtures obtained by XRF are given in Table 2.1
All the mixtures were ball-milled in cyclohexane for 4 hours using agate beads in order to guarantee a good homogeneity.
The dried powders were pre-calcined at 950°C in order to obtain a CO_2-free sample and loaded into platinum capillaries with an inner diameter of 0.52 mm and 0.04 mm thick wall. To suppress the SO_3 evaporation, the platinum capillaries were cap-sealed under vacuum to avoid broken, using an arc sealer.

Table 2.1: Chemical analysis expressed as oxides and chemical modules for all the mixes; Extended uncertainty (U) for X-ray fluorescence analysis results are also reported.

	SiO_2	Al_2O_3	Fe_2O_3	CaO	MgO	SO_3	Na_2O	K_2O	SUM	LSF	AR	SR
U	0.26	0.20	0.10	0.40	0.24	0.16	0.08	0.12				
MIX1	23.02	6.27	3.13	67.42	<0.24	<0.16	<0.08	<0.12	99.85	91.25	2.00	2.45
MIX2	22.96	6.22	3.13	66.82	<0.24	0.70	<0.08	<0.12	99.85	90.70	1.99	2.45
MIX3	22.82	6.19	3.12	66.32	<0.24	1.45	<0.08	<0.12	99.89	90.57	1.98	2.45
MIX7	23.29	4.98	4.41	67.18	<0.24	<0.16	<0.08	<0.12	99.86	90.83	1.13	2.48
MIX8	23.03	4.94	4.38	66.86	<0.24	0.72	<0.08	<0.12	99.92	91.38	1.13	2.47
MIX9	22.82	4.80	4.34	66.47	<0.24	1.49	<0.08	<0.12	99.92	91.85	1.11	2.50
MIX13	23.20	4.96	4.39	66.90	0.42	<0.16	<0.08	<0.12	99.86	90.83	1.13	2.48
MIX14	23.08	4.93	4.37	66.58	0.90	<0.16	<0.08	<0.12	99.86	90.83	1.13	2.48
MIX15	22.97	4.91	4.35	66.25	1.38	<0.16	<0.08	<0.12	99.86	90.83	1.13	2.48

2.2 Data collection

High-resolution X-ray powder diffraction data were collected on beamline ID31 at the European Synchrotron Radiation Facility (ESRF), in Grenoble, France [6]. A wavelength of 0.3264 Å (35 KeV) was chosen to minimize absorption effect due to the platinum capillary. An optical furnace

comprising three 150-W halogen lamps was used to heat the sample up to a maximum temperature of 1500 °C [7].
The temperature in the furnace was changed varying the voltage of the halogen lamps.
The furnace focuses to a zone of 4 mm length along the sample axis, and thus, no direct measurement of the focal point temperature during the data collection is possible. For this reason, the temperature in the furnace was estimated by using the platinum capillary as internal standard, having known thermal expansion coefficients.
The temperature was so deduced by detecting the position of platinum Bragg peaks, in particular the platinum 002 peak, and using the values of thermal expansion coefficients from the literature.
For each experiment, a preliminary fast collection was performed in order to set the voltage corresponding to the maximum temperature (1500 °C). In fact, from one experiment to another, no constant correspondence between voltage applied and temperature measured was observed, for problems related to the ageing of the lamps.
For one sample, SO_3 and MgO free, data were collected during the heating period from room temperature to the maximum temperature and then during the cooling period down to 1200 °C with temperature steps of about 50 °C, with the aim to simulate an industrial process (Fig. 2.1).
Data relating to all the other were collected from the maximum temperature down to 1200 °C with temperature steps of about 25 °C. The collection time was of about 20 minutes for each temperature with an angular range from 3 to 28°2Θ with steps of 2°2Θ.
The XRD powder patterns were analyzed by Rietveld method, using the TOPAS software (vers. 2.1) [8] (see Fig. 2.2).

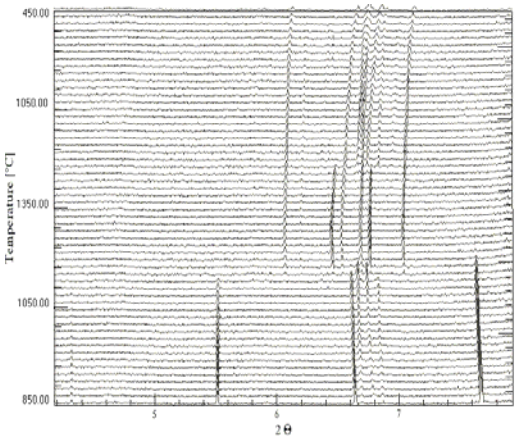

Fig. 2.1 X-ray patterns collected at different temperatures, upon heating and cooling of sample MIX4.

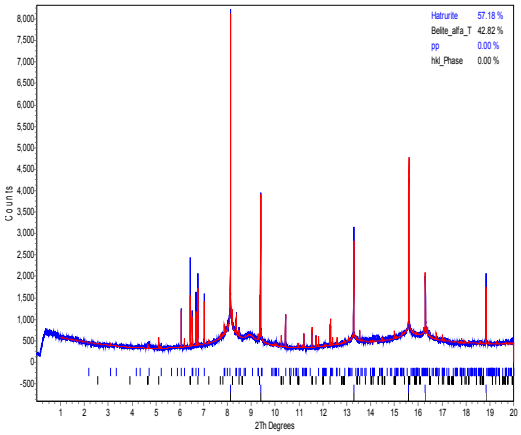

Fig. 2.2 Example of a refinement. Blue line is the observed pattern; red line is the calculated one. Vertical bars indicate the position of the Bragg peaks for the phases. Bragg-peaks from Pt-capillary are also marked.

The algorithm which holds for quantitative phase analysis using the Rietveld method (RQPA) is based upon the normalization equation $\sum_i X_i = 1$, where X_i is the weight fraction of component i in the mixture. The application of this equation could bring to overestimate the phase content when an amorphous component is present, as for example a glassy phase produced by the fast cooling of the melt formed at the clinkering temperature.
To compare the weight fractions of C_3S and C_2S in presence of a liquid phase to their weight fractions below the invariant point (i.e. when all liquid phase is crystallized), data were rescaled taking into account the liquid content formed at the different temperatures calculated according to the studies on the quaternary system CaO-Al_2O_3-Fe_2O_3-SiO_2 [5].

3 Results and discussion

Fig. 3.1 shows the calculated weight fractions variation for the phases in sample MIX4, upon heating up to maximum temperature (1500°C) and upon cooling down to temperatures below the invariant point (1338 °C). During the heating process, CaO and Quartz react progressively to form α'-C_2S that reaches its maximum content at about 1200°C. At temperatures above 900 °C, also C_3A starts to form. The phase transition of C_2S from polymorph α' (orthorhombic) to α (rhombohedral) starts at about 1200°C, and at 1300 °C it is completed.
The C_3S was detected at a temperature greater than 1300 °C. This temperature should correspond to the liquid appearance, in agreement with literature data [9]. An acceleration of the C_3S formation was observed when temperature increases in the range 1300-1350°C.
The C_3S content increases less during the cooling step, reaching its maximum content just before the temperature of the invariant point.
When cooling is performed in the temperature range from 1332 to 1274 °C, the aluminate phases (C_3A and C_4AF) start to appear and a huge decrease in C_3S content is observed.
A decreasing C_3S content was observed in samples MIX1 and MIX4, having a composition in terms of Al_2O_3/Fe_2O_3 ratio respectively higher and equal to the Al_2O_3/Fe_2O_3 ratio of 1.38 (see Fig. 3.2). Such a decrease is justified by the peritectic reaction $L+C_3S \rightarrow C_2S+C_3A$ occurring in these mixtures at the invariant point.

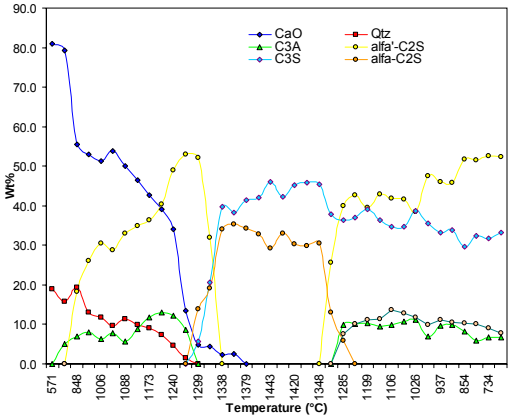

Fig. 3.1: Variation in the phase content, as obtained by RQPA, during the cycle of heating and cooling of the sample MIX4.

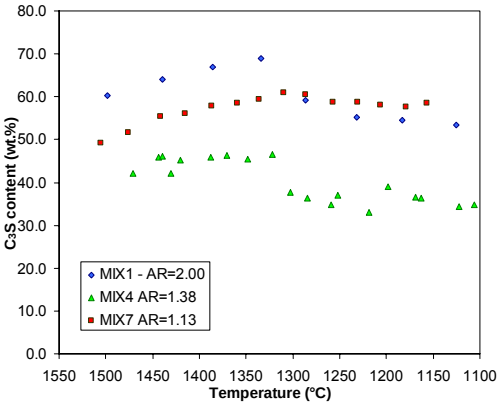

Fig. 3.2: C_3S content variation when cooling MIX1 (Al_2O_3/Fe_2O_3 wt. ratio = 2.00), MIX4 (Al_2O_3/Fe_2O_3 wt. ratio = 1.38) and MIX7 (Al_2O_3/Fe_2O_3 = 1.15).

The decrease in C_3S content was not observed for sample MIX7, having a liquid composition with an Al_2O_3/Fe_2O_3 ratio lower than that of the invariant point. In this situation, according to the phase diagram, the peritectic reaction is $L + C_2S \rightarrow C_3S + C_4AF$.

At the same temperature range of appearance of aluminate and ferrite phases, the C_2S polymorph transition from α to α' occurs.

This phase transition is a rapid and reversible semi-reconstructive transformation and it is characterized by a rotation of half of the SiO_4^{4-} tetrahedra with a consequent change in the Ca-coordination. The temperature of this phase transition is 100 °C lower than that given in the literature [9].

The cell parameters of α'-C_2S polymorph vary as a function of the temperature. This result is clearly apparent when observing the change in the slope at about 1060 °C of the curve in Fig. 3.3 showing the variation for lattice constant *a* as a function of the temperature .

This is clearly an indication of a second-order transition, as the polymorphic transition $\alpha'_H \rightarrow \alpha'_L$ is.

This transition is an order-disorder transformation of very small amplitude that causes only a small displacement of the calcium atoms that involves a superstructure. In fact this transformation causes the lattice parameter *a* to triple..

The attempt of including the $Pna2_1$ super-structure in the refinements for temperatures lower than 1060°C instead of the α'_H model failed to lead to proper improvements in terms of refinement agreement factors (R_{wp} = 12.80% and 12.76% for Pnma and $Pna2_1$ respectively). This is probably due to the high similarity of this two polymorphs; in fact the model proposed for α'_L form is strictly related to the disordered Pnma structure of α'_H. Moreover as for the α to α'_H phase transition, the temperature at which the phase transition α'_H to α'_L occurs is about 100°C lower than the one found in the literature [9].

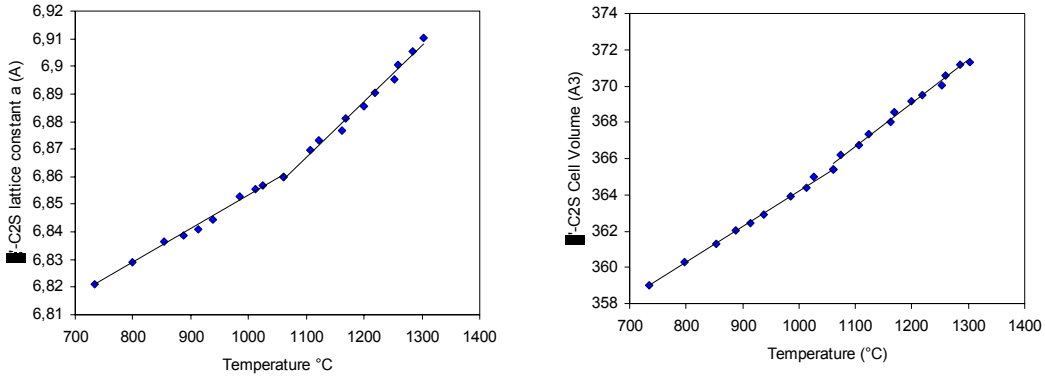

Fig. 3.3 Thermal expansion of α'-C_2S in MIX4. The change in the slope for the lattice constant a and for the cell volume between 1100 and 1000 °C is apparent..

3.1 SO_3 effect

Fig. 3.4 shows the plot of the C_3S/C_2S wt. ratio obtained during the cooling from the maximum temperature of three different samples, having the same basic composition but different SO_3 contents (see Table 2.1). The increasing SO_3 content in the sample causes the C_3S/C_2S wt. ratio to decrease in the equilibrium clinker composition at 1500°C. The C_3S/C_2S ratio varies from 2.5 for the sample without SO_3 to less than 1 for the sample with 1.5% of SO_3. No Bragg peaks due to CaO (free lime) were detected in the X-ray diffraction patterns for all the samples at the maximum temperature, so the decrease in the C_3S/C_2S ratio cannot be attributed to a defective equilibrium.
In the samples having an SO3 content in the 0 to 0.75% range, the C_3S/C_2S ratio slightly increases up to the invariant point and, at the time the aluminate phases are formed, a huge decrease is observed.
In the sample with 1.5% of SO_3, the C_3S/C_2S wt. ratio decreases during cooling.
The presence of SO_3 influences the C_3S/C_2S wt. ratio considerably and brings about a slight decrease in the temperature at which aluminate phases are formed (see Fig. 3.9).
If the variations of cell parameters during cooling (see Fig. 3.6 and 3.7) in samples containing different amount of SO_3 are compared, it is possible to observe an increase in the C_2S cell volume, while the variation in the C_3S cell volume is quite negligible. This is an indirect confirmation of the fact that SO_3 goes in the silicate structure and preferentially in C_2S rather than in C_3S.
Data from SEM-EDS analysis conducted on the same sample confirm this observation (see Fig. 3.5).

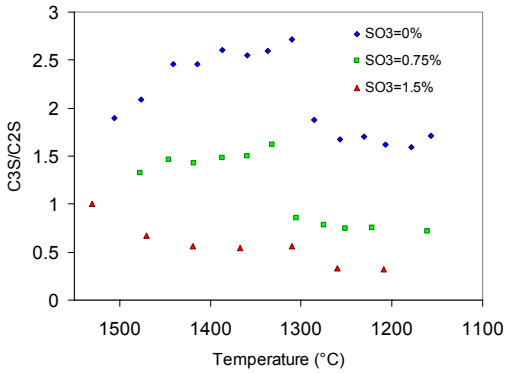

Fig. 3.4: RQPA C_3S/C_2S wt. ratio variation when cooling samples containing different amounts of SO_3

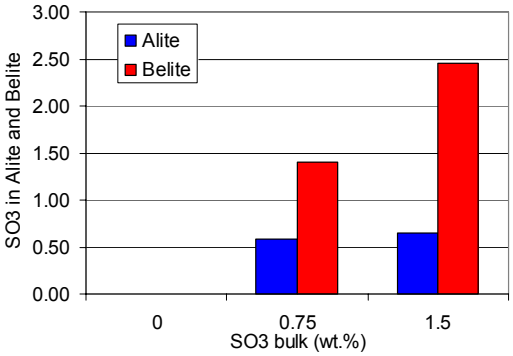

Fig. 3.5: SEM-EDS results for alite and belite in samples containing different amounts of SO_3

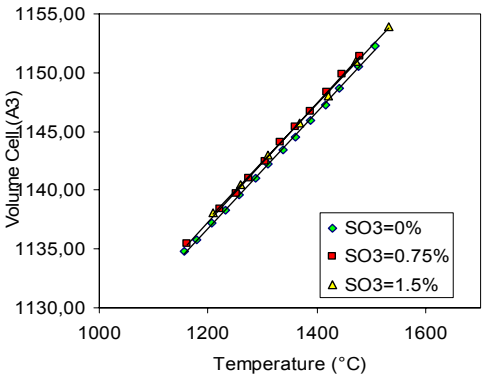

Fig. 3.6 C_3S thermal expansion in samples with different amount of SO_3.

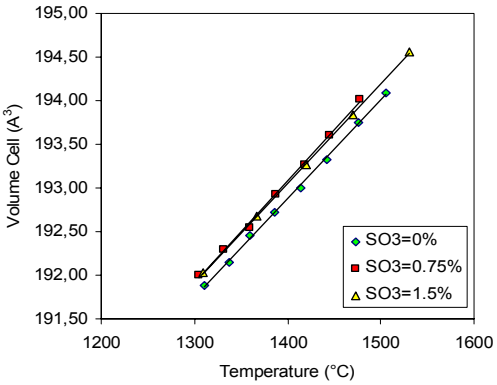

Fig. 3.7: α-C_2S thermal expansion in samples with different amount of SO_3.

The thermal expansion coefficients for C_3S and C_2S have been calculated also by regression analysis of the volume cell data as a function of the temperature in order to evaluate their variation with increasing SO_3 contents.
The values of the thermal expansion coefficients so calculated for C_3S and C_2S in the different mixtures are reported in Table 3.1.

Table 3.1 Linear thermal expansion coefficient of alite and belite for samples containing different amounts of SO_3. Errors are reported in brackets.

	C_3S	C_2S
	α_v (/°C)	α_v (/°C)
MIX7 (SO_3 =0%)	4.34(6)E-05	5.86(16)E-05
MIX8 (SO_3 =0.75%)	4.44(8)E-05	6.04(22)E-05
MIX9(SO_3 =1.5%)	4.32(10)E-05	5.93(10)E-05

No significant change in the linear thermal expansion coefficients for both alite and belite has been observed as a function of the SO_3 content of the mix. The values given in Table 3.2 are within the limits of the error of the regression equation.

3.2 MgO effect

Fig. 3.8 shows the plot of the C_3S/C_2S wt. ratio recorded when cooling the samples with the same composition in terms of main oxides but with different MgO contents (see Table 2.1). The C_3S/C_2S wt. ratio increases from 2.5 in the sample without MgO to 3.5 in the sample with 0.5% MgO. In the sample containing 1.5% of MgO, the C_3S/C_2S ratio reduces to 1.5.
The C_3A/C_4AF wt. ratio decreases with increasing MgO contents. Only the sample containing 1.5% of MgO seems to behave differently, as the higher C_3A/C_4AF wt. ratio indicates.

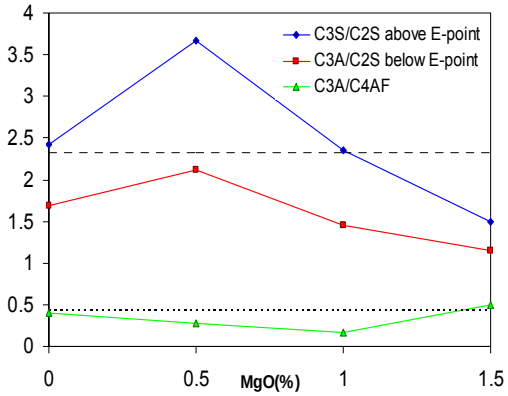

Fig. 3.8: C_3S/C_2S and C_3A/C_4AF wt. ratio variation as a function of the MgO content. Dashed lines represent the values calculated from the theoretical composition.

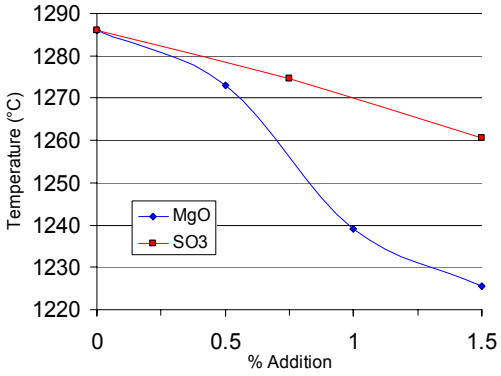

Fig. 3.9 Temperature at which aluminate phases have been first detected in the X-ray pattern for samples with different additions of MgO and SO_3.

The presence of MgO produces significant reduction in the invariant point temperature as the decreasing temperature of aluminate phase formation in the samples containing MgO demonstrates (see Fig 3.9).
The C_3S cell volume decreases with increasing total MgO contents.
A variation in C_2S cell volume is observed only for sample containing 1.5% of MgO. This is an indirect confirmation of the fact that Mg substitutes Ca ions preferentially into the C_3S structure rather than into the C_2S one. Only for high MgO contents, possibly when the solid solution limit is reached, some Mg ions go into C_2S.
Data from SEM-EDS analysis conducted on the same samples confirm this observation.

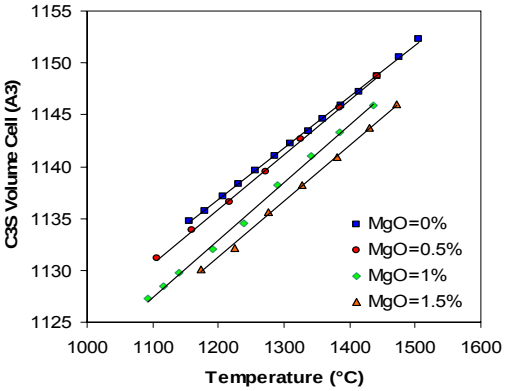

Fig. 3.9: C_3S thermal expansion in samples with different amount of MgO.

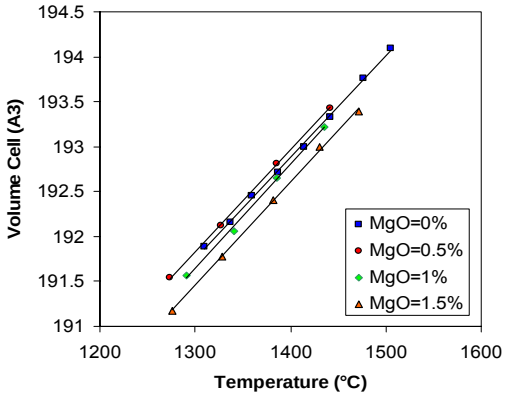

Fig. 3.10: α-C_2S thermal expansion in samples with different amount of MgO.

The thermal expansion coefficients for C_3S and C_2S have also been calculated in order to evaluate their variation with increasing MgO contents.

The linear thermal expansion coefficients, calculated for C_3S and C_2S of the different mixes, are given in Table 3.2.

An increase in the linear thermal expansion coefficients as a function of MgO content of the mix is observed for C_3S (from 4.34E-05 to 4.86E-05) while no variation in the thermal expansion coefficient for C_2S is found.

Table 3.2: Linear thermal expansion coefficient of alite and belite for samples containing different amounts of MgO. Errors are given in brackets.

	C3S	C_2S
	α_v (/°C)	α_v (/°C)
MIX7 (MgO =0 wt.%)	4.34(6)E-05	5.86(16)E-05
MIX13 (MgO =0.5 wt. %)	4.62(10)E-05	5.88(12)E-05
MIX14 (MgO=1.0 wt. %)	4.86(16)E-05	6.02(25)E-05
MIX15(MgO =1.5 wt %)	4.75(20)E-05	5.99(20)E-05

4 Conclusions

The application of “in-situ” high-temperature X-ray diffraction for investigating the equilibrium phase diagrams of interest to cement production has been shown to offer new insights into this field, being a time-saving tool compared to quenching methods as well as a more rigorous method with respect to actual operating conditions. It has been possible to follow the high temperature reactions and the crystallization path of clinker phases while they were occurring at the clinkering temperatures.

The results obtained on mixtures featuring the typical clinker Portland composition are in agreement with the deductions based on the fundamental phase diagram [1].

The application of RQPA analysis on HTXRD data yielded useful information about the influence of SO_3 and MgO on the phase equilibrium in the quaternary system related to the OP clinker formation.
Main conclusions can be summarized as follow:

1. The C_3S/C_2S ratio decreases as SO_3 increases in the mixtures, while aluminate total content and C_3A/C_4AF wt. ratio tends to decrease. These results confirm the previous observations made on industrial clinkers [4].
2. The temperature of the invariant point is slightly reduced with increasing SO_3 contents.
3. The C_2S cell volume increases when SO_3 is present. Nevertheless, no variation in its thermal expansion coefficients has been observed.
4. The C_3S/C_2S ratio shows a maximum value in correspondence of an MgO content of 0.5%. Moreover, the MgO content has a limited influence on the C_3A/C_4AF ratio.
5. The temperature of the invariant point considerably decreases with increasing MgO contents, thus confirming all previous observations [1].
6. The C_3S cell volume reduces with increasing MgO contents in the mixtures; therefore, a slight change in its thermal expansion coefficients has been observed.

References

[1] Lea's, Chemistry of Cement and Concrete, 4th ed., Edward Arnold Ltd., England, 1998
[2] S. Uda, E. Asakura and M. Nagashima, Influence of SO_3 on the Phase Relationship in the System $CaO-SiO_2-Al_2O_3-Fe_2O_3$, J. Am. Ceram. Soc., 81(3) (1998) 725-729
[3] H.F.W. Taylor, "Distribution of sulphate between phases in Portland cement clinkers", Cem. Concr. Res., 29, (1989), 1173-1179
[4] U. Costa and M. Marchi "Mineralogical composition of clinker by Bogue and Rietveld method: The effect of minor elements. Proceedings of the 11th ICCC (2003) 151-159.
[5] F.M. Lea and T.W. Parker, The quaternary system $CaO-Al_2O_3-SiO_2-Fe_2O_3$ in relation to cement technology Building Research Technical Paper, 16, London: H.M.S.O. (1935), 52 pp
[6] A.N. Fitch, The High Resolution Powder Diffraction Beam Line at ESRF, J. Res. Natl .Inst. Stand. Technol., 109, (2004), 133-142
[7] S.M. Moussa, R.M Ibberson, M. Bieringer, A.N. Fitch and M.J. Rosseinsky, In situ Measurement of Cation Order and Domain Growth in an Electroceramic, Chem. Mater., 15, (2003), 2527-2533.
[8] Bruker AXS, TOPAS V2.1: General profile and structure analysis software for powder diffraction data. - User manual, Bruker AXS, (2003), Karlsruhe, Germany.
[9] H.F.W. Taylor, Cement Chemistry, Academic Press, New York, 1990